Journal of Organometallic Chemistry 694 (2009) 150–156

Contents lists available at ScienceDirect

Journal of Organometallic Chemistry

journal homepage: www.elsevier.com/locate/jorganchem

A novel series of iridium complexes with alkenylquinoline ligands: Theoretical study on electronic structure and spectroscopic property

Tao Liu [a], Xin Zhou [a], Qing-Jiang Pan [b], Bao-Hui Xia [a,c], Hong-Xing Zhang [a,*]

[a] State Key Laboratory of Theoretical and Computational Chemistry, Institute of Theoretical Chemistry, Jilin University, Changchun 130023, PR China
[b] Laboratory of Physical Chemistry, School of Chemistry and Materials Science, Heilongjiang University, Harbin 150080, PR China
[c] College of Chemistry, Jilin University, Changchun 130023, PR China

ARTICLE INFO

Article history:
Received 2 September 2008
Received in revised form 8 October 2008
Accepted 14 October 2008
Available online 22 October 2008

Keywords:
Iridium(III) complexes
Excited state
Spectroscopic properties
DFT

ABSTRACT

The ground and the lowest-lying triplet excited state geometries, electronic structures, and spectroscopic properties of a novel series of neutral iridium(III) complexes with cyclometalated alkenylquinoline ligands [(C^N)$_2$Ir(acac)] (acac = acetoylacetonate; C^N = 2-[(*E*)-2-phenyl-1-ethenyl]pyridine (pep) **1**; 2-[(*E*)-2-phenyl-1-ethenyl]quinoline (peq) **2**; 1-[(*E*)-2-phenyl-1-ethenyl]isoquinoline (peiq) **3**; 2-[(*E*)-1-propenyl]pyridine (pp) **4**; 2-[(*E*)-1-fluoro-1-ethenyl]pyridine (fpp) **5**) were investigated by DFT and CIS methods. The highest occupied molecular orbital is composed of *d*(Ir) and π(C^N) orbital, while the lowest unoccupied molecular orbital is dominantly localized on C^N ligand. Under the TD-DFT with PCM model level, the absorption and phosphorescence in CH_2Cl_2 media were calculated based on the optimized ground and triplet excited state geometries, respectively. The calculated lowest-lying absorptions at 437 nm (**1**), 481 nm (**2**), 487 nm (**3**), 422 nm (**4**), and 389 nm (**5**) are attributed to a {[$d_{x^2-y^2}$(Ir) + d_{xz}(Ir) + π(C^N)] → [π^*(C^N)]} transition with metal-to-ligand/intra-ligand charge transfer (MLCT/ILCT) characters, and the calculated phosphorescence at 582 nm (**1**), 607 nm (**2**), 634 nm (**3**), 515 nm (**4**), and 491 nm (**5**) can be described as originating from the ^{3}{[$d_{x^2-y^2}$(Ir) + d_{xz}(Ir) + π(C^N)] [π^*(C^N)]} excited state with the ^{3}MLCT/^{3}ILCT characters. The calculated results revealed that the phosphorescent color of these new Ir(III) complexes can be tuned by changing the π-conjugation effect strength of the C^N ligand.

1. Introduction

Recently, tremendous efforts have been focused on the phosphorescent organic light-emitting devices (OLEDs) through either the design of new materials or the improvements of device structures [1,2]. Because the phosphorescent OLEDs have higher internal quantum efficiency (more than 75%) compared with the fluorescent ones in ideal condition (25%) [3], they are currently a considerable active area of research as a result of the potential application in flat-displays [4]. The transition metal complexes, such as Os(II), Pt(II), Ru(III), and Ir(III) with d^6/d^8 electronic configuration, have been widely employed as phosphorescent emitters in OLEDs because these complexes are able to harvest both triplet and singlet excitons due to the strong spin–orbit coupling, which in turn increases the efficiency of intercrossing of the emitting triplet excited state [5,6]. Among these heavy metal complexes, Ir(III) complexes are the most effective, tunable, and sublimable phosphorescent material for OLEDs fabrication [7,8].

On experiment, since it was reported that OLEDs prepared with Ir(ppy)$_3$ (ppy = 2-phenylpyridine) have greater efficiencies more than 80%, Ir(III) complexes have attracted much more attention [9–20]. Numerous homoleptic and heteroleptic cyclometalated Iridium complexes, emitting from blue to red, such as Ir(C^N)$_3$, Ir(C^N)$_2$L, and IrLL' have been synthesized and their spectral properties have been investigated by Thompson [9,10,21], Collin [22,23], and Slugovc [24] experimentally. The iridium complexes with polymer ligands were extensively studied by Cao and coworkers [25,26]. All of them concluded that the emission color can be changed by adjusting the substituent and π-electron effect of the ligands, namely, tuning the energy levels of the highest occupied molecular orbital (HOMO) and the lowest occupied molecular orbital (LUMO).

Previous theoretical investigations showed that the HOMO is dominantly composed of *d*(Ir) and π(ligand), and the LUMO is localized on ligands, so the lowest-lying absorption is always assigned to metal-to-ligand charge transfers (MLCT), ligand-to-ligand charge transfer (LLCT), intra-ligand charge transfer (ILCT), and mixing transitions of MLCT/LLCT/ILCT. Furthermore, the theoretical work proved that the emission color can be tuned by changing HOMO–LUMO gap and helped to design new luminescent Ir complexes with high efficiency [11,27–30].

* Corresponding author. Tel.: +86 431 88498966; fax: +86 431 88945942.
E-mail addresses: liutao@email.jilu.edu.cn (T. Liu), zhanghx@mail.jlu.edu.cn (H.-X. Zhang).

0022-328X/$ - see front matter © 2008 Elsevier B.V. All rights reserved.
doi:10.1016/j.jorganchem.2008.10.022

Table 1
The main optimized geometry structural parameters of the complexes in the ground and the lower-lying triplet excited state at the B3LYP and CIS level, respectively, together with the experimental values of $(tpy)_2Ir(acac)$.

Parameters	1		2		3		4		5		Expt.[a]
	X^1A	A^3B	X1A	A^3B	X^1A	A^3B	X^1A	A^3B	X^1A	A^3B	
Bond length (Å)											
Ir–N	2.062	2.087	2.102	2.130	2.063	2.086	2.067	2.092	2.076	2.096	2.040(5)
Ir–C	2.020	2.055	2.010	2.046	2.012	2.046	2.010	2.035	1.971	2.006	1.985(7)
Ir–O	2.189	2.182	2.198	2.182	2.187	2.173	2.199	2.191	2.175	2.160	2.161(4)
Bond angle (°)											
N–Ir–N	179.5	179.0	179.1	179.2	179.7	179.3	177.0	176.7	174.6	174.3	176.2(2)
O–Ir–O	85.4	82.7	84.0	82.1	85.3	83.1	84.7	82.4	85.6	83.3	88.2(2)
C–Ir–C	98.6	99.5	99.0	99.2	98.9	98.4	92.1	90.9	93.4	92.2	
Dihedral angel (°)											
C(2)–C(3)–C(4)–C(5)	133.3	142.4	138.3	142.2	135.5	134.8					
C(6)–N–Ir–O	80.3	81.8	75.2	76.4	79.3	83.0	87.8	91.6	87.5	90.6	

[a] From Ref. [10].

Recently, Cheng and co-workers [31,32] synthesized a new series of iridium complexes containing cyclometallated alkenylpyridines ligands, they also investigated the absorption and emission spectra, and applied these iridium complexes in OLEDs. The phosphorescence color of these cyclometallated alkenylpyridines iridium complexes can be changed by tuning the alkenylpyridine ligand structure easily. And the devices based on these iridium complexes emit highly saturated red light with the external quantum efficiency, brightness, and Commission Internationale de L'Eclairage (CIE) coordinates among the best reported so far. But the theoretical study from an electronic structure point of view on the spectral properties and the relation between alkenylpyridine ligand and the spectra is sparse.

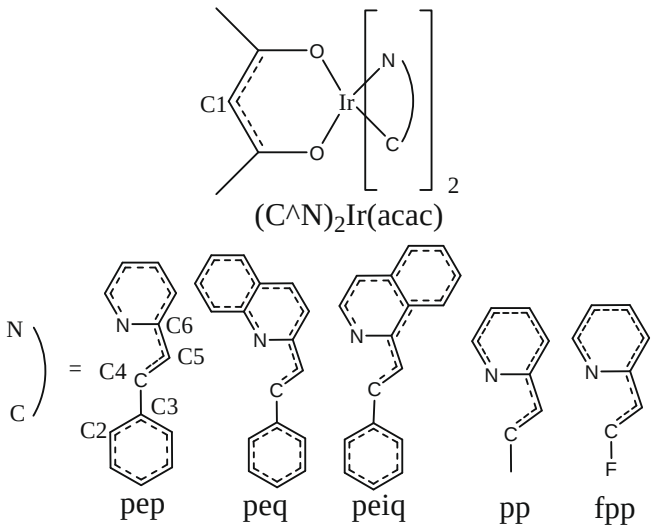

Fig. 1. The optimized geometries of **1–5** at B3LYP/LANL2DZ level.

Using above background, we carried out the present work, aimed at providing an in-depth theoretical understanding of the electronic structures and spectroscopic properties of a novel series of alkenylpyridines Ir(III) complexes $[(C^N)_2Ir(acac)]$ [31,32] (acac = acetoylacetonate; C^N = 2-[(*E*)-2-phenyl-1-ethenyl]pyridine (pep), **1**; 2-[(*E*)-2-phenyl-1-ethenyl]quinoline (peq), **2**; 1-[(*E*)-2-phenyl-1-ethenyl]isoquinoline (peiq), **3**; 2-[(*E*)-1-propenyl]pyridine (pp), **4**; 2-[(*E*)-1-fluoro-1-ethenyl]pyridine (fpp), **5**). Highly importantly, the effects of the peripheral alkenylpyridines ligand on the phosphorescence were revealed so that the phosphorescent color can be tuned by adjusting alkenylpyridines ligands.

2. Computational details

Density functional theory [33] (DFT) with Becke's three parameter functional and the Lee–Yang–Parr functional [34] (B3LYP) and configuration interaction with single-excitations [35–37] (CIS) approaches were employed to optimize ground and excited state geometries. Based on the optimized ground and excited state geometries, the absorption and emission properties were calculated by the time-dependent DFT [38–40] (TDDFT) method. Initial optimized calculations were performed in the absence of solvent. Then, to simulated the effect of solution by dichloromethane (CH_2Cl_2), the single point TDDFT calculations (50 excited states) were repeated using the polarized continuum model (PCM) [41,42]. This kind of theoretical approach has been proven to be reliable for transition metal complex systems [28–30,43,44].

In the calculations, a 'double-ζ' quality basis set consisting of Hay and Wadt's [45,46] effective core potentials (LANL2DZ) was employed for Ir atoms, and an all-electron 6-31 G basis set for the no-metal atoms (H, C, N, O and F). A relativistic effective core potential (ECP) replaced the inner core electrons of the Ir(III) element, leaving the outer core ($5s^25p^6$) electrons and the $5d^6$ valence electrons. The basis sets were described as Ir (8s6p3d/3s3p2d), C, N, O, and F (10s4p/3s2p), and H (4s/2s). Thus, 391 basis functions

Table 2
Molecular orbital compositions (%) of $(pep)_2Ir(acac)$ (**1**) in the ground state.

Orbital	*E*/(eV)	Ir	Acac	Pep	Bond type	Ir component
L + 4 69a	−0.51			94.2	π^*_s(pep)	
L + 3 66b	−0.54			97.0	π^*(pep)	
L + 1 67a	−1.20			86.7	π^*_s(pep)	
L 65b	−1.30			88.6	π (pep)	
HOMO–LUMO energy gap						
H 66a	−4.86	37.0		57.9	*d*(Ir) + π(pep)	26.8 $d_{x^2-y^2}$ 8.7 d_{xz}
H-1 64b	−5.39	43.0	33.4	23.6	*d*(Ir) + π(acac) + π(pep)	39.5 d_{yz}
H-2 63b	−5.62		13.1	81.4	π(acac) + π(pep)	
H-3 65a	−5.89	70.4		23.3	*d*(Ir) + π(pep)	62.5 d_{z^2}

Table 3
Molecular orbital compositions (%) of $(peq)_2Ir(acac)$ (**2**) in the ground state.

Orbital	*E*/(eV)	Ir	Acac	Peq	Bond type	Ir component
L + 4 82a	−0.57			95.4	π^*(peq)	
L + 3 79b	−0.72			97.8	π^*(peq)	
L + 1 80a	−1.66			90.1	π^*(peq)	
L 78b	−1.68			90.1	π (peq)	
HOMO–LUMO energy gap						
H 79a	−4.92	32.4		64.3	*d*(Ir) + π(peq)	22.7 $d_{x^2-y^2}$ 7.8 d_{xz}
H-1 77b	−5.36	35.9	24.9	39.2	*d*(Ir) + π(acac) + π(peq)	34.4 d_{yz}
H-2 76b	−5.56		27.9	64.9	π(acac) + π(peq)	
H-3 78a	−5.90	52.6		42.1	*d*(Ir) + π(peq)	46.5 d_{z^2}
H-11 74a	−6.86		15.0	74.1	π(acac) + π(peq)	

and 260 electrons for **1**, 471 basis functions and 312 electrons for **2** and **3**, 293 basis functions and 196 electrons for **4**, 281 basis functions and 196 electrons for **5** were included in the calculations. All of the calculations were accomplished by using the GAUSSIAN 03 software package [47] on an IBM server.

The calculated complexes display C_2 symmetry in both of the ground and excited states. The *z*/C_2 axis orients through Ir and the central C(1) atom in the acac cycle, and the *y* axis go though N, Ir, N atoms. Under the C_2 symmetry, the total molecular orbitals of **1**–**5** were divided into 'a' and 'b' irreducible orbitals.

3. Results and discussion

3.1. The ground and the triplet excited states geometries and the vibrational frequencies

The important ground state optimized geometry parameters together with the X-ray crystal diffraction data of $[(tpy)_2Ir(acac)]$ (tpy = 2-(4-tolyl)pyridine) [10] for comparison are listed in Table 1 and the optimized geometries are shown in Fig. 1. The calculated results revealed that **1**–**5** have X^1A ground state. Vibrational frequencies were calculated based on the optimized geometries of **1**–**5** to verify that each of the geometries is a minimum (no imaginary frequency) on the potential energy surface.

The optimization results showed that the two alkenylquinoline ligands are almost perpendicular to acac ligand with the C(6)–N–Ir–O dihedral angle close to 90°. The phenyl substituents are not coplanar to the ethenyl group (C=C) of the C^N ligand because the C(2)–C(3)–C(4)–C(5) dihedral angle of **1**–**5** are among 130–140°, which is consistent with the conclusion obtained by Cheng [31]. Furthermore, it can be seen that the optimized bond lengths and bond angles of **1**–**5** in the ground state are in general agreement with the corresponding experimental values of $[(tpy)_2Ir(acac)]$ [10]. Take **1** for example, the calculated bond distances of Ir–N (2.062 Å), Ir–C (2.020 Å), and Ir–O (2.189 Å) are overestimated by less than 0.03 Å compared with the measured values, but consistent with our previous calculated results of $[(tpy)_2Ir(acac)]$ [28]. The calculated bond angles are closed to the experimental values with a deviation less than 3.0° [10].

The partial frontier molecular orbital compositions and energies of **1**–**5** involving in excitations are given in Tables 2–6 which show that **1**–**5** have the similar frontier molecular orbital compositions. The HOMOs of **1**–**5** are dominantly composed of $d_{x^2-y^2}$(Ir), d_{xz}(Ir), and π (C^N), while the LUMOs are dominantly localized on C^N ligand, the other low unoccupied molecular orbital are all composed of π^*(C^N) or π^*(acac) without *d*(Ir). Tables 2–6 also show that the composition of the frontier molecular orbitals are hardly changed by tuning π conjugation length of C^N ligands, but the HOMO–LUMO gaps of **1**–**5** are increased in the order of **3** (3.20 eV) < **2** (3.24 eV) < **1** (3.56 eV) < **4** (3.74 eV) < **5** (3.96 eV) due to different C^N ligand, which is consistent with the reverse order of π-conjugation effect of C^N ligands peiq (**3**) > peq (**2**) > pep (**1**) > pp (**4**) > fpp (**5**).

Table 4
Molecular orbital compositions (%) of $(peiq)_2Ir(acac)$ (**3**) in the ground state.

Orbital	*E*/(eV)	Ir	Acac	Peip	Bond type	Ir component
L + 8 81b	0.24			94.9	π^*(peiq)	
L + 6 83a	−0.23			96.8	π^*(peiq)	
L + 3 82a	−0.61			95.7	π^*(peiq)	
L + 1 80a	−1.61			88.8	π^*(peiq)	
L 78b	−1.70			90.8	π (peiq)	
HOMO–LUMO energy gap						
H 79a	−4.90	32.2		64.0	*d*(Ir) + π(peiq)	21.9 $d_{x^2-y^2}$ 9.1 d_{xz}
H-1 77b	−5.32	31.2	16.7	52.1	*d*(Ir) + π(acac) + π(peiq)	25.8 d_{yz}
H-2 76b	−5.59	17.4	34.6	48.0	*d*(Ir) + π(acac) + π(peiq)	14.6d_{yz}
H-10 72b	−6.77	10.6	43.4	46.0	*d*(Ir) + π(acac) + π(peiq)	

Table 5
Molecular orbital compositions (%) of $(pp)_2Ir(acac)$ (**4**) in the ground state.

Orbital	*E*/(eV)	Ir	Acac	Pp	Bond type	Ir component
L + 4 50b	−0.36			97.5	π^*(pp)	
L + 3 53a	−0.45			95.0	π^*(pp)	
L + 1 51a	−1.00		21.9	71.5	π^*(acac) + π^*(pp)	
L 49b	−1.07			89.9	π (pp)	
HOMO–LUMO energy gap						
H 50a	−4.82	43.5		51.2	*d*(Ir) + π(acac) + π(pp)	28.7 $d_{x^2-y^2}$ 12.4 d_{xz}
H-1 48b	−5.33	47.3	38.5	14.2	*d*(Ir) + π(acac) + π(pp)	38.7d_{yz}
H-2 47b	−5.68			94.8	π(pp)	
H-3 49a	−5.77	71.8		21.8	*d*(Ir) + π(pp)	45.1d_{z^2} 23.9 d_{xz}

Table 6
Molecular orbital compositions (%) of $(fpp)_2Ir(acac)$ (**5**) in the ground state.

Orbital	E/(eV)	Ir	Acac	Fpp	Bond type	Ir component
L + 4 53a	−0.59			94.9	π^*(fpp)	
L + 1 51a	−1.27		26.5	67.2	π^*(acac) + π^*(fpp)	
L 49b	−1.36			89.0	π (fpp)	
HOMO–LUMO energy gap						
H 50a	−5.32	36.6		58.3	d(Ir) + π(fpp)	25.5 $d_{x^2-y^2}$ 8.9 d_{xz}
H-1 48b	−5.82	31.8	55.7	12.5	d(Ir) + π(acac) + π(fpp)	26.5 d_{yz}
H-2 47b	−6.02			94.4	π(fpp)	
H-3 49a	−6.58	71.6		20.8	d(Ir) + π(fpp)	45.8 d_{z^2} 24.7 d_{xz}
H-5 45b	−7.05	20.0	58.4	21.6	d(Ir) + π(acac) + π(fpp)	16.4 d_{yz}

The main geometry parameters of **15** in the A^3B excited state obtained by CIS method are also listed in Table 1. In the low-lying triplet excited state, the geometries of **15** do not vary notably relative to those in the ground state except that the Ir–N, Ir–C, and Ir–O bond lengths change slightly and the four complexes show the similar variation trend. The calculated Ir–C and Ir–N bond lengths relax 0.025 Å and 0.035 Å, respectively, but the Ir–O bond length is strengthened less than 0.020 Å, which indicates that the C^N ligands have a trend to break away from Ir center but the acac ligand is getting closed in the excited state. The calculated O–Ir–O bond angle is reduced by 2.0–3.0°, while N–Ir–N and C–Ir–C bond angles are hardly changed by excitation. In triplet excited state, the phenyl groups of **1** and **2** have a trend to increase the π-conjugation because the C(2)–C(3)–C(4)–C(5) dihedral angles are increased by about 10° compared with those in ground state. The slight difference of the geometry structures result from the electron transition from Ir–C^N bonding orbital to π^*(C^N) orbital (vide infra) upon excitation.

4. Absorption in CH_2Cl_2 media

The calculated absorptions in the UV–visible region associated with their oscillator strengths, main configuration, and the assignments as well as the experimental results are summarized in Table 7. The fitted Gaussian type absorption curves are shown in Fig. 2.

Table 7
The calculated absorptions of **1**–**5** with TDDFT method, together with the experimental values.

	Transition	Configuration (|CI|)	E/nm (eV)	Oscillator	Transition nature	λ_{exptl}/nm (eV)[a]
Singlet → singlet						
1	X1A → A^1B	66a → 65b (0.66)	437 (2.83)	0.1577	MLCT/ILCT	464 (2.67)
	X^1A → B^1B	64b → 67a (0.66)	370 (3.35)	0.0370	MLCT/LLCT/ILCT	395 (3.14)
	X^1A → C^1B	63b → 67a (0.63)	324 (3.83)	0.2536	ILCT	318 (3.90)
	X^1A → D^1B	65a → 66b (0.45)	269 (4.61)	0.4246	MLCT/ILCT	
		63b → 69a (0.36)			ILCT	
2	X^1A → A^1B	79a → 78b (0.67)	481 (2.58)	0.2153	MLCT/ILCT	510 (2.43)
	X^1A → B^1B	77b → 80a (0.65)	418 (2.97)	0.0442	MLCT/LLCT/ILCT	425 (2.92)
	X^1A → C^1B	76b → 80a (0.66)	372 (3.33)	0.2141	LLCT/ILCT	340 (3.65)
	X^1A → D^1B	77b → 82a (0.53)	299 (4.15)	0.1386	MLCT/LLCT/ILCT	
	X^1A → E^1B	74a → 78b (0.38)	271 (4.57)	0.1949	ILCT	
		78a → 79b (0.38)			MLCT/ILCT	
3	X^1A → A^1B	79a → 78b (0.67)	487 (2.51)	0.2824	MLCT/ILCT	510 (2.43)
	X^1A → B^1B	77b → 80a (0.63)	412 (3.01)	0.0519	MLCT/LLCT/ILCT	425 (2.92)
	X^1A → C^1B	76b → 80a (0.64)	364 (3.41)	0.3130	MLCT/LLCT/ILCT	340 (3.65)
	X^1A → D^1B	77b → 82a (0.59)	301 (4.12)	0.2933	MLCT/LLCT/ILCT	
	X^1A → E^1B	72b → 80a (0.43)	274 (4.53)	0.2186	LLCT/ILCT	
		77b → 83a (0.31)			MLCT/LLCT/ILCT	
		79a → 81b (0.29)			MLCT/ILCT	
4	X^1A → A^1B	50a → 49b (0.68)	422 (2.94)	0.0896	MLCT/ILCT	457 (2.71)
	X^1A → B^1B	48b → 51a (0.62)	359 (3.46)	0.0257	MLCT/LLCT/ILCT	377 (3.29)
	X^1A → C^1B	49a → 49b (0.53)	321 (3.86)	0.2679	MLCT/ILCT	321 (3.86)
		50a → 50b (0.36)			MLCT/ILCT	
	X^1A → D^1B	48b → 53a (0.52)	297 (4.17)	0.1046	MLCT/LLCT/ILCT	
	X^1A → E^1B	47b → 53a (0.57)	265 (4.69)	0.1745	ILCT	
5	X^1A → A^1B	50a → 49b (0.68)	389 (3.19)	0.1428	MLCT/ILCT	
	X^1A → B^1B	48b → 51a (0.63)	331 (3.74)	0.0399	MLCT/LLCT/ILCT	
	X^1A → C^1B	49a → 49b (0.64)	288 (4.30)	0.1598	MLCT/ILCT	
	X^1A → D^1B	45b → 51a (0.49)	249 (4.97)	0.2606	LLCT/ILCT	
		47b → 53a (0.31)			ILCT	
Singlet → triplet						
1	X^1A → A^3B	66a → 65b (0.68)	542 (2.28)		^{3}MLCT/^{3}ILCT	
2	X^1A → A^3B	79a → 78b (0.66)	600 (2.07)		^{3}MLCT/^{3}ILCT	
3	X^1A → A^3B	79a → 78b (0.66)	625 (1.98)		^{3}MLCT/^{3}ILCT	
4	X^1A → A^3B	50a → 49b (0.66)	501 (2.48)		^{3}MLCT/^{3}ILCT	
5	X^1A → A^3B	50a → 49b (0.65)	474 (2.62)		^{3}MLCT/^{3}ILCT	

[a] From Refs. [31,32]

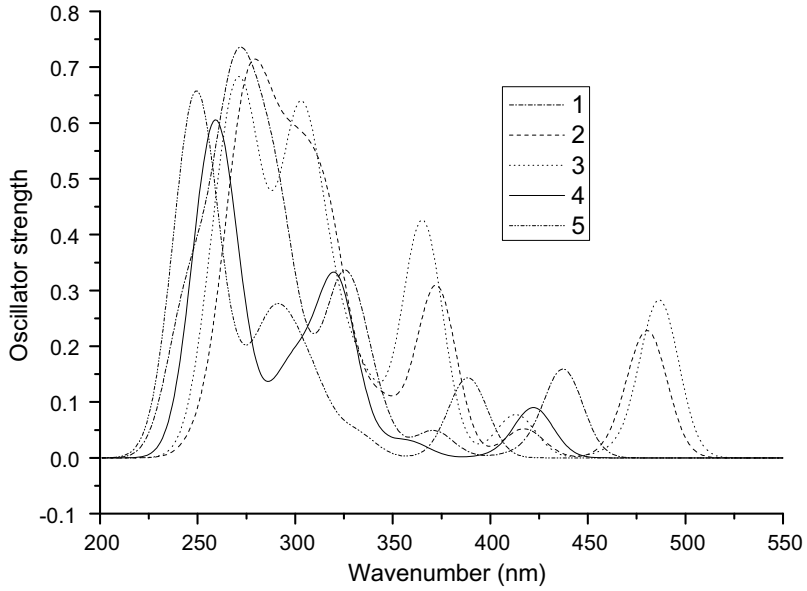

Fig. 2. The simulated absorption spectra of **1–5** in CH_2Cl_2 media.

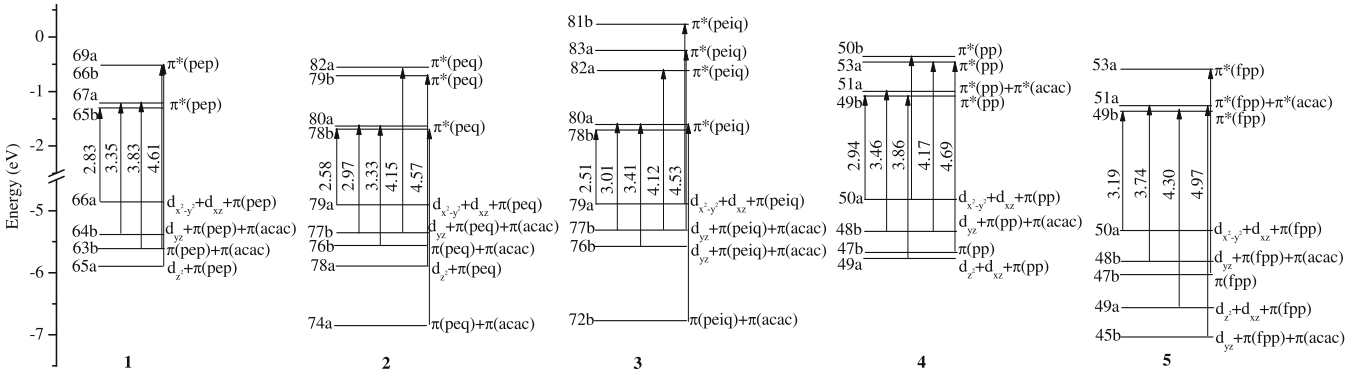

Fig. 3. Diagrams of the molecular orbitals related to in the absorptions for **1–5.**

To intuitively understand the transition process, the molecular orbital energy levels of **15** involved in excitations are displayed in Fig. 3.

Fig. 2 and Table 7 show that the lowest-lying distinguishable absorption bands of **15** are at 437 nm (2.83 eV), 481 nm (2.58 eV), 487 nm (2.51 eV), 422 nm (2.94 eV), and 389 nm (3.19 eV), these calculated absorption bands can be regarded as the measured absorptions of **1**, **2**, **3** and **4** at 464 nm (2.67 eV), 510 nm (2.43 eV), 510 nm (2.43 eV), and 457 (2.71 eV) nm, with a deviation by about 0.2 eV [31,32]. Table 7 shows that excitation of HOMO (66a) → LUMO (65b) with the configuration coefficient of 0.66 is responsible for the absorption band of **1** at 437 nm. Table 2 shows that MO 66a is composed of 26.8% $d_{x^2-y^2}$(Ir), 8.7% d_{xz}(Ir), and 57.9% π(C^N), while MO 65b is dominantly localized on pep ligand. Thus, the lowest-lying absorption at 437 nm is assigned to $\{[d_{x^2-y^2}(\mathrm{Ir}) + d_{xz}(\mathrm{Ir}) + \pi\ (\mathrm{pep})] \rightarrow [\pi^*(\mathrm{pep})]\}$ transition with MLCT and ILCT transition character. From Table 27, we can see that the lowest-lying absorption of **15** have the similar MLCT/ILCT transition characters because of the similar HOMO and LUMO compositions. The excitation energies of **15** are increased in the order of **3** (2.51 eV) < **2** (2.58 eV) < **1** (2.83 eV) < **4** (2.94 eV) < **5** (3.19 eV), which is also consistent with the reverse order of π-conjugation effect of C^N ligand, peiq (**3**) > peq (**2**) > pep (**1**) > pp (**4**) > fpp (**5**), just like the order of HOMO–LUMO gap. Furthermore, the whole absorption curves of **15** are obviously red shifted by increasing the π-conjugation effect of C^N ligand.

Table 7 shows that the high energy absorption bands of **15**, between 4.53 eV and 4.97 eV, have $^1A \rightarrow {}^1B$ transition character. With respect to **1**, the two excitations of MO 65a → MO 66b (|CI| = 0.45) and MO 63b → MO 69a (|CI| = 0.36) contribute to the absorption at 269 nm. Table 2 shows that the occupied MO 65a has 62.5% d_{z^2}(Ir), and 23.3% π(pep), MO 63b is dominantly contributed by π(pep) orbital, while both of the unoccupied MOs 66b and 69a are localized on pep ligand. Thus this high energy absorption at 269 nm can be assigned to MLCT mixed with ILCT transition. Interestingly, we found the ILCT composition is getting great and the MLCT composition is getting small with the increase of the π-conjugation effect of C^N ligand **1** < **2** < **3**. But with respect to **4** and **5**, this high energy absorption is dominantly contributed by ILCT excitation.

The other absorption bands showed in Fig. 2 are all attributed to different MLCT (including $d_{x^2-y^2}$(Ir), d_{yz}(Ir), d_{z^2}(Ir) and d_{xz}(Ir) orbitals), LLCT, and ILCT or the mixing excitations. The LLCT and the ILCT transitions are assigned to $[\pi(\mathrm{acac}) \rightarrow \pi^*(\mathrm{C^N})]$ and $[\pi(\mathrm{C^N}) \rightarrow \pi^*(\mathrm{C^N})]$. The second and the third absorption bands at 370 and 324 nm (**1**), 418 and 372 nm (**2**), 412 and 364 nm (**3**), 359 and 321 nm (**4**) are consistent with the experiment results

Table 8
The calculated and the corresponding experimental emissions of **15**.

	Transition	Config. (CI coeff.)	λ/nm (eV)	Transition nature	Expt./nm (eV)[a]
1	A3B → X^1A	65b → 66a (0.69)	582 (2.13)	^{3}MLCT/^{3}ILCT	616 (2.01)
2	A^3B → X^1A	78b → 79a (0.67)	607 (2.04)	^{3}MLCT/^{3}ILCT	638 (1.94)
3	A^3B → X^1A	78b → 79a (0.66)	634 (1.95)	^{3}MLCT/^{3}ILCT	664 (1.87)
4	A^3B → X^1A	49b → 50a (0.66)	515 (2.41)	^{3}MLCT/^{3}ILCT	536 (2.31)
5	A^3B → X^1A	49b → 50a (0.65)	491 (2.53)	^{3}MLCT/^{3}ILCT	

[a] From Refs. [31,32].

Table 9
Molecular orbital compositions (%) of 15 in the A^3B excited states.

	Orbital	E/(eV)	Ir	C^N	Bond type	Ir component
1	L 65b	−1.30		88.6	π(C^N)	
	H 66a	−4.86	37.0	57.9	$d_{x^2-y^2}$ + d_{xz} + π(C^N)	26.8 $d_{x^2-y^2}$ 7.7 d_{xz}
2	L 78b	−1.67		90.4	π(C^N)	
	H 79a	−4.90	32.7	63.2	$d_{x^2-y^2}$ + d_{xz} + π(C^N)	23.0 $d_{x^2-y^2}$ 8.1 d_{xz}
3	L 78b	−1.72		91.7	π(C^N)	
	H 79a	−4.88	33.7	61.2	$d_{x^2-y^2}$ + d_{xz} + π(C^N)	23.1 $d_{x^2-y^2}$ 8.3 d_{xz}
4	L 49b	−1.08		89.8	π(C^N)	
	H 50a	−4.78	42.3	51.3	$d_{x^2-y^2}$ + d_{xz} + π(C^N)	28.3 $d_{x^2-y^2}$ 11.6 d_{xz}
5	L 49b	−1.36		88.6	π(C^N)	
	H 50a	−5.29	35.5	58.6	$d_{x^2-y^2}$ + d_{xz} + π(C^N)	24.6 $d_{x^2-y^2}$ 8.9 d_{xz}

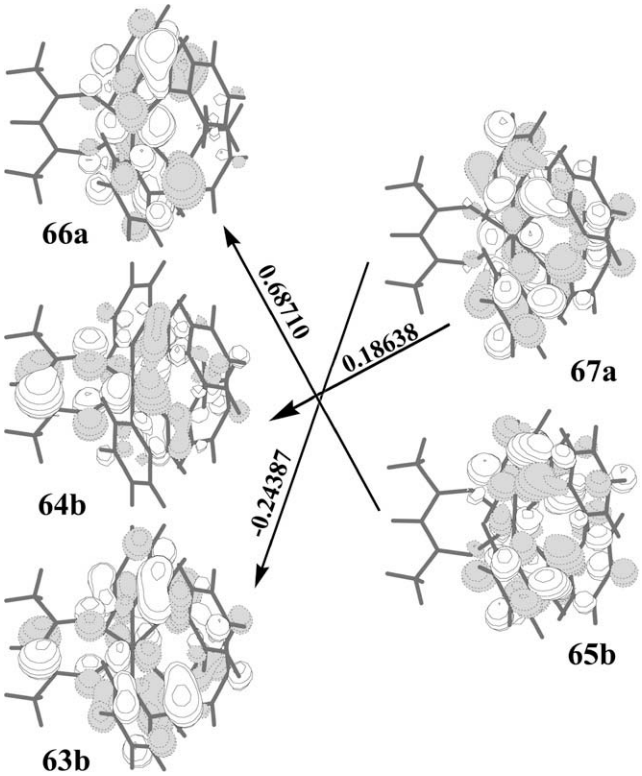

Fig. 4. Single electron transition with |CI coefficients| > 0.1 under TD-DFT calculation for the 582 nm emission of $(pep)_2Ir(acac)$ (**1**) in CH_2Cl_2 media.

with a deviation about 0.2 eV, which indicated that our calculated absorption results are reasonable and acceptable [31,32]. Table 7 also shows that the calculated vertical triplet absorptions of **1**, **2**, **3**, **4**, and **5** at 542 nm (2.28 eV), 600 nm (2.07 eV), 625 nm (1.98 eV), 501 nm (2.48) and 474 nm (2.62 eV), respectively, and these triplet absorptions have the similar ^{3}MLCT/^{3}ILCT transition characters to the lowest-lying singlet absorptions.

5. Emission in CH_2Cl_2 media

The calculated phosphorescence of **1–5** in CH_2Cl_2 media and the measured emissions are summarized in Table 8. The frontier molecular orbitals compositions responsible for the emissions are compiled in Table 9.

The calculated phosphorescence of **1**, **2**, **3**, **4** and **5** at 582 nm (2.13 eV), 607 nm (2.04 eV), 634 nm (1.95 eV), 515 nm (2.41 eV), and 491 nm (2.53 eV) agree well with the experimental results [31,32] of **1**, **2**, **3**, and **4** at 616 (2.01 eV), 638 (1.94 eV), 664 (1.87 eV), and 536 (2.31 eV) nm, respectively, with a deviation about 0.1 eV, which indicated that our calculated emission result is reasonable and acceptable. With respect to **1**, three transitions of MO 65b → MO 66a (0.69), MO 63b → MO 67a (0.24), and MO 64b → MO 67a (0.19) should be responsible for the emission at 582 nm. Owing to the large difference of CI coefficient among them, the assignment of the lowest-lying emission should correspond to the MO 65b → MO 66a transition. Table 9 shows that MO 66a, −4.863 eV, is composed of 26.8% $d_{x^2-y^2}$(Ir), 7.7% d_{xz}(Ir), and 57.9% π(pep), while MO 65b, −1.30 eV, is dominantly contributed by π^*(pep) orbital. Thus the emission of **1** at 582 nm can be described as originating from the ^{3}{[$d_{x^2-y^2}$(Ir) + d_{xz}(Ir) + π(pep)] [π^*(pep)]} excited state with the ^{3}MLCT/^{3}ILCT character. The electron density diagram for emission 582 nm of **1** is shown in Fig. 4 to help to understand the emissive process from the $A^3B \rightarrow X^1A$ transition intuitively. Tables 8 and 9 show that the triplet excited states of **2**–**5** have similar ^{3}MLCT/^{3}ILCT character to that of **1**.

The calculated results revealed that the lowest-lying singlet (triplet) absorptions of **1** – **5** are all dominantly arise from the combination of MLCT/ILCT (^{3}MLCT/^{3}ILCT) electronic transition, which is the reverse process of the phosphorescence because of the same symmetry and the transition characters.

With respect to **2** and **3**, the absorption and the emission spectra are all red-shifted by increasing the π-conjugation of C^N ligand compared with **1**. Although the absorptions of **2** and **3** have similar red-shifted extent by about 0.3 eV compared with that of **1**, the emission of them are different. The emission of **2** is red-shifted by about 0.2 eV, while that of **3** is red-shifted by ca. 0.3 eV, which results from the orientation of the increased π-conjugation effect. The π-conjugation of **2** is strengthened on the direction perpendicular with the N–Ir–N direction, while that of **3** is increased on the N–Ir–N direction which is easy for the transition between ^{3}MLCT excited state and the ground state result in small transition energy. It is consistent with the Pt complexes investigated by Chou and Chi [48]. With respect to **4** and **5**, the absorption and the emission spectra are blue-shifted replacing $-C_6H_5$ by $-CH_3$ and –F, which is because the π-conjugation effect is reduced. Moreover, the LUMO of **4** is raised and the HOMO of **5** is stabilized compared with **1**.

In order to verify the rationality of such CIS and TD-DFT combined calculations, we optimized the structures of **1**–**4** in the triplet excited states using the UB3LYP method. Their emission energies were predicted at the TD-DFT level. The excited-state geometry parameters, the properties of emission and the component of MOs are listed in Tables S1–S3 (Supplementary material). It was shown that the electronic excitation slightly changes the geometry structures in the UB3LYP optimizations, similar to the case in the CIS. Compared with corresponding experimental values,

the emission energies of **1**–**4** systematically were underestimated in the UB3LYP/TD-DFT calculations but overestimated in the CIS/TD-DFT. These results agree with previous reports [49,50]. In the present work, we mainly discussed CIS/TDDFT results.

6. Conclusions

The present work have investigated the ground and excited states geometries, absorption and phosphorescence properties of five Iridium(III) complexes with C^N (pep, peq, peiq, pp, and fpp) and acac ligands theoretically. The *d*(Ir) orbital composition of HOMO can be changed by altering C^N ligands, but the LUMO is hardly influenced. The lowest-lying absorptions of **1**–**5** are all assigned to MLCT/ILCT mixing transition, and the phosphorescence of them can be described as originating from ^{3}MLCT/^{3}ILCT excited state. The emission color can be tuned by changing π -conjugation strength of the C^N ligands and adding electron-withdrawing/electron-donating groups on C^N ligands. So it is very practical to explore the relation between C^N and phosphorescence. We hope these theoretical studies can provide suggestion in designing highly efficient phosphorescent materials.

Acknowledgments

This work was supported by the Natural Science Foundation of China (Grant Nos. 20573042, 20703015 and 20333050).

Appendix. Supplementary material

Tables S1–S3, giving the triplet excited state geometry parameter, emission results, and the excited state frontier molecular orbital composition of **1**–**4** obtained by UB3LYP/TD-B3LYP methods. Supplementary data associated with this article can be found, in the online version, at doi:10.1016/j.jorganchem.2008.10.022.

References

[1] R.F. Friend, R.W. Gymer, A.B. Holmes, J.H. Burroughes, R.N. Marks, C. Taliani, D.C. Bradley, D.A. Dos Santos, J.L. Bredas, M. Loglund, W.R. Salaneck, Nature 397 (1999) 121.
[2] A.J. Heeger, Angew. Chem., Int. Ed. 40 (2001) 2591.
[3] C. Adachi, M.A. Baldo, S.R. Forrest, M.E. Thompson, Appl. Phys. Lett. 77 (2000) 904.
[4] Y. Wand, N. Herron, V.V. Grushin, D.D. LeCloux, V.A. Petrov, Appl. Phys. Lett. 79 (2001) 449.
[5] V. Balzani, A. Juris, M. Venturi, S. Campagna, S. Serroni, Chem. Rev. 96 (1996) 759.
[6] D. Amarante, C. Cherian, A. Catapano, R. Adams, M.H. Wang, E.G. Megehee, Inorg. Chem. 44 (2005) 8804.
[7] W.Y. Wong, G.J. Zhou, X.M. Yu, H.S. Kwok, Z.Y. Lin, Adv. Funct. Mater. 17 (2007) 315.
[8] W.Y. Wong, C.L. Ho, Z.Q. Gao, B.X. Mi, C.H. Chen, K.W. Cheah, Z.Y. Lin, Angew. Chem., Int. Ed. 45 (2006) 7800.
[9] S. Lamansky, P. Djurovich, D. Murphy, F. AbdelRazzaq, H.E. Lee, C. Adachi, P.E. Burrows, S.R. Forrest, M.E. Thompson, J. Am. Chem. Soc. 123 (2001) 4304.
[10] S. Lamansky, P. Djurovich, D. Murphy, F. AbdelRazzaq, R. Kwong, I. Tsyba, M. Bortz, B. Mui, R. Bau, M.E. Thompson, Inorg. Chem. 40 (2001) 1704.
[11] P.J. Hay, J. Phys. Chem. A 106 (2002) 1634.
[12] J.P.J. Markham, S.C. Lo, S.W. Magennis, P.L. Burn, I.D.W. Samuel, Appl. Phys. Lett. 80 (2002) 2645.
[13] J.W. Hu, G.H. Zhang, H.H. Shih, X.Q. Jiang, P.P. Sun, C.H. Cheng, J. Organomet. Chem. 693 (2008) 2798.
[14] M.A. Baldo, S. Lamansky, P.E. Burrows, M.E. Thompson, S.R. Forrest, Appl. Phys. Lett. 75 (1999) 4.
[15] C.H. Yang, K.H. Fang, W.L. Su, S.P. Wang, S.K. Su, I.W. Sun, J. Organomet. Chem. 691 (2006) 2767.
[16] W.S. Sie, J.Y. Jian, T.C. Su, G.H. Lee, H.M. Lee, K.B. Shiu, J. Organomet. Chem. 693 (2008) 1510.
[17] C.H. Yang, C.C. Tai, I.W. Sun, J. Mater. Chem. 14 (2004) 947.
[18] T. Yutaka, S. Obara, S. Ogawa, K. Nozaki, N. Ikeda, T. Ohno, Y. Ishii, K. Sakai, M. Haga, Inorg. Chem. 44 (2005) 4737.
[19] K.A. King, P.J. Spellane, R.J. Watts, J. Am. Chem. Soc. 107 (1985) 1431.
[20] Md.K. Nazeeruddin, R. HumphryBaker, D. Berner, S. Rivier, L. Zuppiroli, M. Graetzel, J. Am. Chem. Soc. 125 (2003) 8790.
[21] A.B. Tamayo, B.D. Alleyne, P.I. Djurovich, S. Lamansky, I. Tsyba, N.N. Ho, R. Bau, M.E. Thompson, J. Am. Chem. Soc. 125 (2003) 7377.
[22] J.P. Collin, I.M. Dixon, J.P. Sauvage, J.A.G. Williams, F. Barigelletti, L. Flamigni, J. Am. Chem. Soc. 121 (1999) 5009.
[23] I.M. Dixon, J.P. Collin, J.P. Sauvage, L. Flamigni, Inorg. Chem. 40 (2001) 5507.
[24] S. Kappaun, S. Sax, S. Eder, K.C. Moller, K. Waich, F. Niedermair, R. Saf, K. Mereiter, J. Jacob, K. Mullen, E.J.W. List, C. Slugovc, Chem. Mater. 19 (2007) 1209.
[25] B. Du, L. Wang, H.B. Wu, W. Yang, Y. Zhang, R.S. Liu, M.L. Sun, J.B. Peng, Y. Cao, Chem. Eur. J. 13 (2007) 7432.
[26] X.H. Li, Z. Chen, Q. Zhao, L. Shen, F.Y. Li, T. Yi, Y. Cao, C.H. Huang, Inorg. Chem. 46 (2007) 5518.
[27] Y.S. Kim, H.L. Young, Curr. Appl. Phys. 7 (2007) 504.
[28] T. Liu, B.H. Xia, X. Zhou, H.X. Zhang, Q.J. Pan, J.S. Gao, Organometallics 26 (2007) 143.
[29] T. Liu, H.X. Zhang, B.H. Xia, J. Phys. Chem. A 111 (2007) 8724.
[30] T. Liu, H.X. Zhang, X. Shu, B.H. Xia, Dalton Trans. (2007) 1922.
[31] B.M.J.S. Paulose, D.K. Rayabarapu, J.P. Duan, C.H. Cheng, Adv. Mater. 16 (2004) 2003.
[32] D.K. Rayabarapu, B.M.J.S. Paulose, J.P. Duan, C.H. Cheng, Adv. Mater. 17 (2005) 349.
[33] E. Runge, E.K.U. Gross, Phys. Rev. Lett. 52 (1984) 997.
[34] A.D. Becke, J. Chem. Phys. 98 (1993) 5648.
[35] J.F. Stanton, J. Gauss, N. Ishikawa, M. HeadGordon, J. Chem. Phys. 103 (1995) 4160.
[36] J.B. Foreman, M. HeadGordon, A. Pople, J. Phys. Chem. 96 (1992) 135.
[37] V.A. Waiters, C.M. Hadad, Y. Thiel, S.D. Colson, K.B. Wibergy, P.M. Johnson, J.B. Foresman, J. Am. Chem. Soc. 113 (1991) 4782.
[38] R.E. Stratmann, G.E. Scuseria, J. Chem. Phys. 109 (1998) 8218.
[39] N.N. Matsuzawa, A. Ishitani, J. Phys. Chem. A 105 (2001) 4953.
[40] M.E. Casida, C. Jamorski, K.C. Casida, D.R. Salahub, J. Chem. Phys. 108 (1998) 4439.
[41] M. Cossi, G. Scalmani, N. Regar, V. Barone, J. Chem. Phys. 117 (2002) 43.
[42] V. Barone, M. Cossi, J. Chem. Phys. 107 (1997) 3210.
[43] M. Sun, B. Niu, J.P. Zhang, Theor. Chem. Acc. 119 (2008) 489.
[44] D.M. Dattelbaum, R.L. Martin, J.R. Schoonover, T.J. Meyer, J. Phys. Chem. A 108 (2004) 3518.
[45] P.J. Hay, W.R. Wadt, J. Chem. Phys. 82 (1985) 299.
[46] P.J. Hay, W.R. Wadt, J. Chem. Phys. 82 (1985) 270.
[47] M.J. Frisch, G.W. Trucks, H.B. Schlegel, G.E. Scuseria, M.A. Robb, J.R. Cheeseman, J.A. Montgomery Jr., T. Vreven, K.N. Kudin, J.C. Burant, J.M. Millam, S.S. Iyengar, J. Tomasi, V. Barone, B. Mennucci, M. Cossi, G. Scalmani, N. Rega, G.A. Petersson, H. Nakatsuji, M. Hada, M. Ehara, K. Toyota, R. Fukuda, J. Hasegawa, M. Ishida, T. Nakajima, Y. Honda, O. Kitao, H. Nakai, M. Klene, X. Li, J.E. Knox, H.P. Hratchian, J.B. Cross, C. Adamo, J. Jaramillo, R. Gomperts, R.E. Stratmann, O. Yazyev, A.J. Austin, R. Cammi, C. Pomelli, J.W. Ochterski, P.Y. Ayala, K. Morokuma, G.A. Voth, P. Salvador, J.J. Dannenberg, V.G. Zakrzewski, S. Dapprich, A.D. Daniels, M.C. Strain, O. Farkas, D.K. Malick, A.D. Rabuck, K. Raghavachari, J.B. Foresman, J.V. Ortiz, Q. Cui, A.G. Baboul, S. Clifford, J. Cioslowski, B.B. Stefanov, G. Liu, A. Liashenko, P. Piskorz, I. Komaromi, R.L. Martin, D.J. Fox, T. Keith, M.A. AlLaham, C.Y. Peng, A. Nanayakkara, M. Challacombe, P.M.W. Gill, B. Johnson, W. Chen, M.W. Wong, C. Gonzalez, J.A. Pople, GAUSSIAN 03, Revision C.02, Gaussian, Inc.: Wallingford, CT, 2004.
[48] S.Y. Chang, J. Kavitha, J.Y. Hung, Y. Chi, Y.M. Cheng, E.Y. Li, P.T. Chou, F.H. Lee, A. Carty, Inorg. Chem. 46 (2007) 7064.
[49] V.I. Stsiapura, A.A. Maskevich, V.A. Kuzmitsky, K.K. Turoverov, I.M. Kuznetsova, J. Phys. Chem. A 111 (2007) 4829.
[50] K.A. Nguyen, P.N. Day, R. Pachter, J. Phys. Chem. A 103 (1999) 9378.